Pergamon

Bioorganic & Medicinal Chemistry, Vol. 3, No. 6, pp. 861–872, 1995

0968-0896/95 $9.50 + .00

0968-0896(95)00086-0

Multiple DNA Binding Modes of Anthracene-9-Carbonyl-N^1-Spermine

Alison Rodger,[a]* Steven Taylor,[b] Gareth Adlam,[b] Ian S. Blagbrough[b] and Ian S. Haworth[c]*

[a]*Current address: Department of Chemistry, University of Warwick, Coventry CV4 7AL, U.K. formerly at Physical Chemistry Laboratory, Oxford University, South Parks Road, Oxford OX1 3QZ, U.K.*

[b]*Department of Medicinal Chemistry, School of Pharmacy and Pharmacology, University of Bath, Claverton Down, Bath BA2 7AY, U.K.*

[c]*Department of Pharmaceutical Sciences, University of Southern California, 1985 Zonal Ave., Los Angeles, CA 90033, U.S.A.*

Abstract—The poly(dAdT)$_2$ complex of anthracene-9-carbonyl-N^1-spermine, a spermine derivative terminally substituted with an anthracene moiety, has been studied using fluorescence, linear dichroism, circular dichroism, normal absorption spectroscopy (as a function of temperature) and computer modelling. For comparison, some data are also provided for the same ligand with poly(dGdC)$_2$ and calf thymus DNA. Following detailed fluorescence and CD spectroscopic studies, we propose that anthracene-9-carbonyl-N^1-spermine intercalates in at least two different binding orientations with poly(dAdT)$_2$. Based on computer simulation data, we deduce that the ligand can intercalate from both the minor groove and the major groove. In contrast, intercalation with poly(dGdC)$_2$ probably occurs only from the major groove. At high ligand concentrations, the CD spectra suggest anthracene–anthracene interactions, whilst the LD data point towards a groove-bound anthracene. Again from computer simulations, we propose binding modes consistent with these observations. Other data from the LD spectra suggest a sequential nature to the binding of the ligand to calf thymus DNA, with GC-rich sites being occupied first. At low ligand concentrations, anthracene-9-carbonyl-N^1-spermine is able to stabilize poly(dAdT)$_2$ against thermal decomposition, but not as effectively as spermine. The reverse is found to be true with calf thymus DNA. Both the anthracene-9-carbonyl-N^1-spermine and spermine complexes of poly(dAdT)$_2$ show pre-melt transitions in their melting curves. The anthracene-9-carbonyl-N^1-spermine complex with poly(dAdT)$_2$ also shows a post-melt transition.

Introduction

Polyamines are simple, primarily linear, positively charged organic molecules that are present in prokaryotic and eukaryotic cells.[1,2] The best known members of the class are spermidine (**1**) and spermine (**2**) (Fig. 1). The apparent simplicity of polyamines hides a multitude of *in vivo* and *in vitro* effects which have made these molecules of interest from both a biophysical and a medicinal perspective. A role for polyamines in supporting cell growth has been established,[3,4] but the mechanism of this behaviour is poorly understood. As the amine functions of most naturally occurring polyamines are fully protonated at physiological pH, and a significant percentage of cellular polyamines occur in the nucleus,[5] it has long been believed that interactions between natural polyamines and DNA may have significant consequences *in vivo*. This has been reinforced by the finding that the most effective anti-tumour polyamines are ineffective at condensing DNA *in vitro*[6,7] and there is a growing body of evidence linking polyamines to the stability of chromatin structure.[8–11]

A greater understanding of the *in vivo* roles of nuclear polyamines would be facilitated by an accurate model describing their interaction with DNA. This model would incorporate preferred binding orientations and locations (minor groove, major groove, backbone, etc.), base sequence selectivity, association/dissociation kinetics, equilibrium constants for complex formation, etc. Such a model should be able to describe, at a

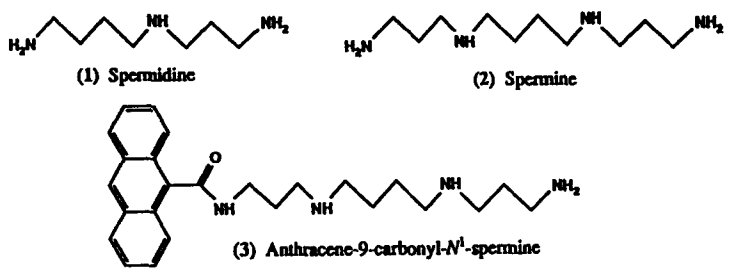

Figure 1. Structures of spermidine (**1**), spermine (**2**) and anthracene-9-carbonyl-N^1-spermine (**3**).

molecular level, the mechanisms through which polyamines modulate DNA conformation.[12,13] In addition, the growing realization of the multi-conformational nature of DNA[14] leads one to speculate that polyamines may have a role in maintaining more esoteric DNA conformations *in vivo*. The earliest and best known example of this is the discovery of left-handed (Z) DNA under non-physiological conditions[15] and the subsequent realization that polyamines stabilize this conformation (*in vitro*) at concentrations similar to those found in cells.[16–18] More recently, triplex DNA, a form of which is now established as an intermediate in chromosomal strand exchange catalyzed by the recA protein,[19] has also been found to be stabilized by polyamines.[20]

X-Ray crystallography has provided some indication of DNA binding sites and Bancroft and co-workers have recently described a spermine binding site with Z-DNA.[21] From similar studies of right-handed helices,[22–24] the variety of polyamine locations and orientations might lead to the conclusion that preferred binding sites do not really exist at all, and that the polyamine–DNA interaction is best described in terms of a general electrostatic interaction. Data from NMR spectroscopy have also been interpreted in terms of a model having no preferred binding sites.[25,26] The difficulty with this conclusion is that numerous studies have shown differences in polyamine binding to DNA duplexes of different sequences.[12,13,27–30] Further, polyamines having the same total charge, but different length alkyl chains, show large variations in their propensity to promote, for example, DNA condensation or formation of left-handed DNA.[4,7,18,31] This is highly suggestive of a structural role, in addition to a general electrostatic role, for polyamines in these processes. Furthermore, this role is likely to depend upon the location of the polyamine on the DNA.

The development of a polyamine–DNA complexation model has been hindered by the 'invisibility' of polyamines to most spectroscopic techniques. This has been addressed by synthesis of spermine derivatives having UV active[27] or photochemically active[29,32] groups. Schmid and Behr, for example, reported a discrimination of spermine for AT-rich minor grooves, using photochemical cleavage experiments with a spermine molecule substituted by a benzenediazonium group.[29]

In synthesizing anthracene-9-carbonyl-N^1-spermine (**3**), we have introduced a substituent onto a terminal amine.[33,34] The anthracene moiety is a poor DNA intercalator,[35] with a binding constant orders of magnitude lower than more effective intercalators; see, for example, the comprehensive review by Denny.[36] Hence the binding of **3** should, in principle, still be dominated by the preferences of the polyamine moiety, at least in terms of groove preference, although some compromise on binding geometry might be expected. We have already shown, from the results of CD experiments at low ligand concentrations, stronger binding of **3** with poly(dGdC)$_2$, compared to poly(dAdT)$_2$.[33] In a previous communication,[34] we described a spectroscopic study of the complex of **3** with calf thymus DNA, showing intercalative binding at low ligand concentration, but some evidence of groove binding of the anthracene moiety at higher concentrations. We also introduced a simple computational approach to study the DNA–ligand complex, and demonstrated that the intercalation event could be simulated using this approach.[34] In this paper, we present the results of a comprehensive spectroscopic study of the complex of **3** with poly(dAdT)$_2$ and complementary fluorescence data for **3** with poly(dGdC)$_2$ and calf thymus DNA. The conclusions from the spectroscopy are complemented with computer modelling data and the proposed binding sites for **3** are then compared with previous studies on the spermine–DNA complex.

Materials

Calf thymus DNA (denoted ctDNA) was purchased from Sigma. Poly(dAdT)$_2$ and poly(dGdC)$_2$ (denoted AT and GC respectively) were obtained from Pharmacia P-L Biochemicals. No further purification was performed. Concentrations were determined spectroscopically using molar extinction coefficients per DNA base of $\varepsilon_{257} = 6600$ for ctDNA, $\varepsilon_{260} = 6600$ for AT and $\varepsilon_{254} = 8400$ for GC. All subsequent references to the DNA concentration refer to the concentration of DNA bases.

Spermidine trihydrochloride (**1**) and spermine tetrahydrochloride (**2**) were purchased from Sigma. Concentrations of **1** and **2** were determined by weight on newly purchased samples. Anthracene-9-carbonyl-N^1-spermine (**3**) was synthesized and purified as previously described.[34] Ethidium bromide was purchased from Aldrich. The concentrations of **3** and ethidium bromide were determined spectroscopically using $\varepsilon_{253} = 110{,}000$ and $\varepsilon_{480} = 5600$ respectively. The 253 nm band of **3** is long axis polarized. All experiments were performed in aqueous solution.

Methods

Fluorescence

The enhancement or quenching of the fluorescence of ligands **3** and ethidium at constant concentrations (of 0.9 μM and 5 μM respectively in 10 mM NaCl), with increasing concentrations of DNA, was determined using a Perkin–Elmer fluorimeter. The exciting wavelength was 370 nm for **3** and 475 nm for ethidium. Emission wavelengths were 440 nm and 595 nm respectively. A titration could not be performed on **3** because it slowly adsorbs onto quartz. Hence, individual solutions of **3** were made at different DNA concentrations. Adsorption was not found to be a problem with ethidium bromide and so the experiment was performed as a titration into the same cell.

Linear dichroism

Flow linear dichroism (LD) measurements were performed on an adapted Jasco J720 spectropolarimeter using a Couette cell described previously.[33] Matching normal absorption experiments were performed on a Cary 3 spectrometer. LD is the differential absorption of light polarized parallel and perpendicular to an orientation direction—in this case the DNA helix axis. LD depends on the isotropic absorbance, A_{iso}, the degree of orientation of the sample, S, and the angle between the polarization of the transition at a particular wavelength, α, as follows:

$$LD = A_{iso} S (3\langle\cos^2\alpha\rangle - 1)$$

where <> denotes averaged over all states. The ratio LD/A_{iso} is often referred to as the reduced linear dichroism, LD^r. The LD^r should be constant across an isolated transition, and two transitions with the same polarization with respect to the DNA helix axis should have the same LD^r values. Thus, the π–π^* transition of a planar aromatic intercalator should have the same LD^r as a DNA base (unless the helix is more or less rigid in the neighbourhood of the intercalator, see below).

Our intention was to determine the effects of **3** on DNA flexibility and/or curvature compared to that of **1** and **2** and also to determine the orientation of **3** when bound to AT and ctDNA. The orientation factor, S, of the DNA, often changes when molecules are bound because the DNA will usually be stiffened or bent to accommodate the ligand. However, S can often be found from the pure DNA transitions, as LD^r is proportional to $3\langle\cos^2\alpha\rangle$ and the π–π^* transitions of planar aromatic intercalators occur within the plane of the molecule and are usually taken to be perpendicular to the DNA helix axis. For **3** this has to be done carefully because its transitions overlap those of DNA. The absorption intensity at 280 nm is due almost entirely to the DNA, so we used the LD^r at that point to determine S. To determine the orientation of **3**, it was also necessary to subtract out the DNA LD to determine the ligand LD, referred to as the LLD. We proceeded by renormalizing the LD, so its S value is the same as that of the pure DNA, in order that the pure DNA spectrum may be subtracted. All spectra are shown as negative LD (–LD) and –LLD to facilitate comparison with normal absorption spectra.

Circular dichroism

Circular dichroism (CD) spectra were measured with a J720 spectrometer.

Computer modelling

In order to understand further the binding modes suggested by the spectroscopic data, we undertook a computer modelling study based on simple molecular dynamics simulations of the ligand–DNA complexes. In performing these simulations, we were able to take advantage of the formal positive and negative charges on the ligand and DNA respectively, such that in a gas phase simulation the components of the complex do not dissociate. The calculation had an initial position of the ligand (or ligands, when multiple ligand–DNA complexes were investigated) about 15 Å from the DNA helix. The ligand was permitted to move towards the helix, and then to move across the surface of the helix, with the motion determined by the appropriate force-field parameters (see below). The helix was retained in a rigid, canonical B-DNA conformation in all the calculations, except that, in certain cases, intercalation sites were built into the structure. These simple calculations proved effective at locating potential ligand binding sites. Of particular interest was that we were able to observe the intercalation of the anthracene moiety during several of the simulations.

All calculations were performed in the AMBER 4.0 force field[37,38] using standard parameters and atomic point charges for the DNA. Point charges for **3** were obtained by first computing an electrostatic potential based on an electron distribution computed in an AM1 calculation,[39] and then backfitting from this potential to a charge distribution, using the program RATTLER.[40] These charges are listed in Table 1. The AM1-minimized structures were also used to derive several other geometrical force-field parameters for the ligands.

The simulations were performed for 400 ps using a long non-bonded cutoff (20 Å) to facilitate the initial approach of the ligand to the helix. As the helix is rigid (and, hence, intra-helix terms are not evaluated) such a cutoff does not result in an excessively computer-intensive simulation. A distance-dependent dielectric of $\varepsilon = 4r_{ij}$ was used to reproduce the shielding of bulk water on the electrostatic interactions. In all simulations, we used alternating 18mer heteropolymer sequences $(dGdC)_9 \cdot (dGdC)_9$ and $(dAdT)_9 \cdot (dAdT)_9$. These duplexes were maintained in either a canonical B-DNA conformation or in a conformation with a centrally placed intercalation site (with a zero helical twist and a 5 Å rise between the base pairs of the intercalation site), in accord with crystal structure data on intercalated DNA–ligand complexes. A third helix, incorporating two such sites between the 4th and 5th, and 14th and 15th base pairs of the 18mer was also used. We note that the intercalation site in the single site helix has a purine-3'-*p*-5'-pyrimidine sequence whilst those in the two site helix have a pyrimidine-3'-*p*-5'-purine sequence.

To obtain some further indication of the stability of binding orientations generated during the molecular dynamics simulations, we selected typical binding modes and subjected them to full energy minimization. These calculations were performed on 14mer duplexes with the ligands centrally bound on the duplex. In the first stage of the calculation the ligand was relaxed and then the entire ligand–DNA complex was subjected to 4000 steps of energy minimization.

Table 1. Point charges (milli-electrons) for anthracene-9-carbonyl-N^1-spermine (3)[a]

atom	charge	atom	charge
Cα	296	C3 (H3)	-87 (87)
C1 (H1)	-234 (121)	C4 (H4)	-283 (162)
C2 (H2)	-60 (111)	N5 (H5)	127 (236)
C3 (H3)	-125 (122)	C6 (H6)	-102 (129)
C4 (H4)	-100 (123)	C7 (H7)	-163 (103)
Cβ	5	C8 (H8)	-139 (105)
C9	-687	C9 (H9)	-137 (141)
C10 (H10)	-152 (145)	N10 (H10)	77 (253)
C	1035	C11 (H11)	-128 (139)
O	-569	C12 (H12)	-139 (103)
N1 (H1)	-802 (325)	C13 (H13)	-120 (144)
C2 (H2)	185 (44)	N14 (H14)	-12 (273)

[a]Atom names for the anthracene moiety follow standard IUPAC nomenclature.[49] Cα and Cβ are bonded to C9 and C10 respectively. The remaining atoms are symmetry related to the atoms shown in the table. The spermine moiety is named N1 to N14 with N1 being the amide nitrogen.

Thermal denaturing studies

Thermal denaturing studies were carried out on the AT and ctDNA complexes of **1**, **2** and **3**. We chose to study a standard system of 200 mM DNA with 20 mM ligand and 10 mM NaCl. The DNA concentration was chosen to optimize spectrometer performance in 5 mm pathlength cells, and the ligand concentration was chosen such that low ligand concentration binding would be present for all systems studied. These experiments were restricted to AT and ctDNA, because, at the salt concentration used, GC does not undergo a helix to coil transition below 100 °C. Measurements were performed using a Cary 3 spectrometer at 270 nm. This wavelength was chosen, rather than the more commonly used 260 nm, in order that **3** would not dominate the absorbance. A wavelength of 280 nm would have been preferable from the viewpoint of the ligand absorbance, but here the change in absorbance with temperature of AT and ctDNA is too small. The temperature was increased at a rate of 0.33 °C min^{-1}, over a range of 25 °C to 98 °C, allowing the system to stabilize for 15 min before taking the first reading. Readings were then taken every minute using a signal averaging time of 2 s.

Results

Fluorescence

The fluorescence of spermine conjugate **3** and ethidium bromide are shown as a function of DNA concentration in Figure 2 (upper and lower panels, respectively). The low DNA concentration parts of the curve (the left hand side) correspond to all DNA sites being occupied; this is referred to as the saturated limit. Conversely, in the high DNA concentration region, each ligand is occupying a most favoured site and the fluorescence observed is referred to as the limiting value of the fluorescence. Significant fluorescence enhancement or quenching is usually associated with intercalative binding so it is these types of binding mode that we are probing with this experiment.

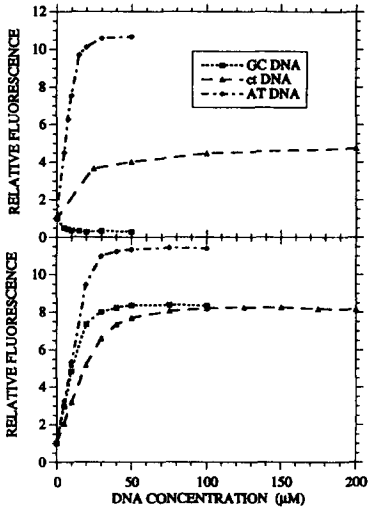

Figure 2. Fluorescence of 0.9 μM anthracene-9-carbonyl-N^1-spermine (**3**) (upper panel) and ethidium bromide (lower panel) in 10 mM NaCl as a function of DNA concentration for GC, AT and ctDNA. Wavelengths are as described in the text.

Ethidium bromide was chosen as a standard for the fluorescence experiments as it has well-characterized intercalation properties and exhibits a large fluorescence enhancement upon intercalation with any DNA sequence (see, for example, Ref. 41). The first part of each curve for ethidium is approximately linear indicating that the relative fluorescence (F/F_o, where F_o is the fluorescence intensity of pure ligand) is directly proportional to the concentration of bound ligand. If we assume that the fluorescence enhancement per ligand when all sites are occupied (low DNA concentration) is the same as when most sites are unoccupied (high DNA concentration), then the average site size, n (in bases), for each bound ligand may be approximately determined from

$$[DNA]/n = \frac{L(1 - F/F_o)}{(1 - (F/F_o)\infty)}$$

where [DNA] is the concentration of DNA bases, F is the fluorescence, L is the ligand concentration, F_o is

the fluorescence intensity of pure ligand and (F/F_o) is the limiting value of the relative fluorescence when all the ligands are bound. The values of n with both AT and GC for ethidium are approximately 4, but the value with ctDNA is about 8, which is not consistent with a nearest neighbour exclusion intercalation model. However, the problem is due to the limiting value of the fluorescence not being appropriate for the saturated binding limit, since all sites are not occupied equally at low ligand concentration. The fluorescence with AT and GC reaches a limiting value by about 50 μM DNA (a DNA base to ligand ratio of 10:1), whereas for ctDNA it requires 100 μM DNA to provide enough optimum sites.

For **3** at the experimental concentration of 0.9 μM, fluorescence enhancement is observed with AT and ctDNA, but quenching occurs with GC (Fig. 2, upper panel). A similar site size analysis as above gives a GC site size for the fluorescence quenching mode of about 7 bases. An approximate binding constant of 1.6×10^7 follows. As the site size previously determined from CD[33] for the most stable binding mode (or modes) was 6 ± 1 with $K = (2.2 \pm 1) \times 10^7$ at 5 mM NaCl, it seems reasonable to conclude that all the ligands bound to GC in sites associated with fluorescence quenching are in a single binding mode. By approximately 10–20 μM DNA (a DNA base to ligand ratio of 10–20:1) a minimum in the fluorescence intensity is reached. Given the values of n and K, this means that if an intercalative site on GC is available, it will be occupied by a ligand, in preference to an alternative binding site. This is in accord with our previous conclusions for this system.[33]

The situation for **3** with AT appears to be more complicated. From the data, we propose a site size different from that found from CD,[33] namely 8.3 ± 1 bases. This discrepancy is explained by the presence of multiple intercalative binding modes having different levels of fluorescence quenching and/or enhancement. The site size from the CD spectra is an average of these multiple modes. Further, the limiting value of the fluorescence is reached at a DNA base to ligand ratio of about 30:1, a rather higher ratio than for the GC–**3** complex. This is perhaps suggestive of a further, non-fluorescence sensitive, binding mode, beginning to occur at higher ligand concentrations.

Linear dichroism

All LD spectra are plotted as –LD or $-LD^r$, so high orientation parallel to the DNA bases corresponds to large positive signals. To provide a contrast with the behaviour of **3**, we first briefly discuss the LD spectra of the DNA complexes of **1** and **2**. Both spermidine **1** and spermine **2** decrease the DNA orientation of ctDNA with the effect of **2** being significantly larger (Fig. 3). Similar results (data not shown) were found with AT and GC. The decrease in orientation observed at lower polyamine concentrations reflects either an increased DNA flexibility (and hence a less effective orientation) or a bending (and hence a shortening) of the DNA. The large orientation loss observed at high concentrations of **2** corresponds to condensation of the DNA.

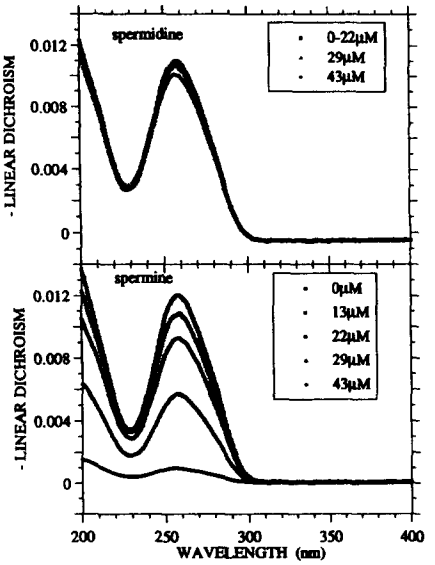

Figure 3. LD spectra of spermidine (upper panel) and spermine (lower panel) complexes with ctDNA. The conditions used were 130 μM ctDNA, 10 mM NaCl and 1 mm pathlength. The DNA base:ligand ratios are given in the figure inserts.

Figure 4 (upper panel) shows the LD for the ctDNA–**3** complex over a similar concentration range to that used in experiments involving **1** and **2**. The LD at 280 nm (where the signal is due only to the DNA bases) indicates the degree of DNA orientation. Low concentrations of **3** decrease the DNA orientation to an extent intermediate between that of **1** and **2**. The rate of decrease in orientation is reduced rather than increased as the ligand concentration increases, until the final spectrum where there actually is an increase in orientation. Figure 5 (upper panel) shows similar data for the AT–**3** complex. Here there is also a change in DNA orientation with ligand binding, but in this case the effect of the ligand is to increase the DNA orientation relative to the free helix, even at low ligand concentrations. Similar experiments for the GC–**3** complex showed a decrease in orientation over the whole concentration range.[33]

The complex of **3** with both ctDNA and AT has a smooth, unstructured LD spectrum at low ligand concentrations (lower panels of Fig. 4 and Fig. 5, respectively). This behaviour also characterizes the GC–**3** complex.[33] At higher ligand concentrations, the LD spectra of the ctDNA–**3** and AT–**3** complexes become increasingly more structured (upper panels of Fig. 4 and Fig. 5, respectively), as do the normal absorption spectra (data not shown). The change corresponds to a new binding mode which occurs once the more favourable binding sites are saturated. The structure in the –LD spectrum includes a dip at 235 nm (ctDNA) or 255 nm (AT), whereas the normal absorption spectra show no such structure at what is, in fact, a maximum. Thus, we can conclude that this new binding mode has a negative $-LD^r$ value (that is, it is

opposite in sign to that of an intercalator). Hence, the ligand is binding in a well defined orientation with the long axis of the anthracene making an angle less than 57.4° with the helix axis, which strongly suggests that it is groove bound.

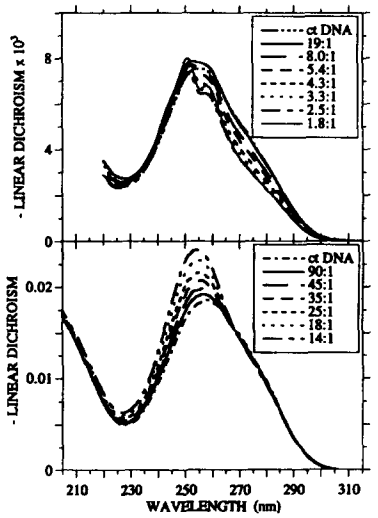

Figure 4. LD spectra of anthracene-9-carbonyl-N^1-spermine–ctDNA complexes at low (upper panel) and high (lower panel) DNA base to ligand ratios. The spectra in each panel were obtained in separate experiments using, for the spectra in the upper panel, 130 μM ctDNA and, for those in the lower panel, 180 μM ctDNA. In each case solutions were 5 mM in NaCl and 1 mm pathlengths were used. The DNA base:ligand ratios are given in the figure inserts.

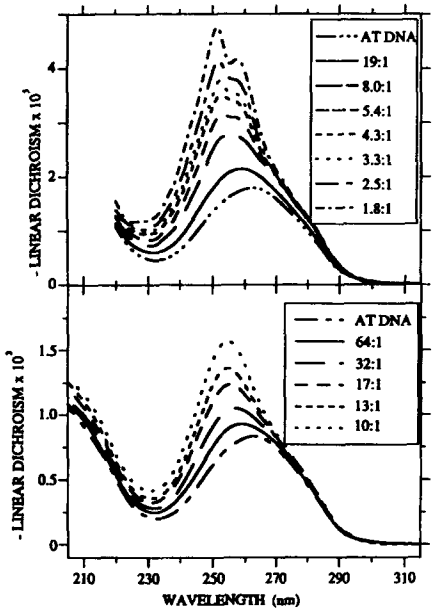

Figure 5. LD spectra of anthracene-9-carbonyl-N^1-spermine–AT complexes at low (upper panel) and high (lower panel) DNA base to ligand ratios. The spectra in each panel were obtained in separate experiments using, for the spectra in the upper panel, 130 μM AT and, for those in the lower panel, 115 μM AT. In each case solutions were 5 mM in NaCl and 1 mm pathlengths were used. The DNA base:ligand ratios are given in the figure inserts.

Circular dichroism

The CD spectra shown in Figure 6 are the CD of **3** plus AT minus the pure AT spectrum. These are best described as induced CD (ICD) spectra since not only does the DNA induce CD intensity into the ligand transitions, but the presence of the ligand also affects the DNA CD, as shown by the non-zero intensity at 280 nm where the ligand has no transitions. The DNA ICD is due either to coupling between DNA and ligand transitions or a change in the DNA base couplings due to a geometry change following ligand binding. In fact, both factors probably contribute.

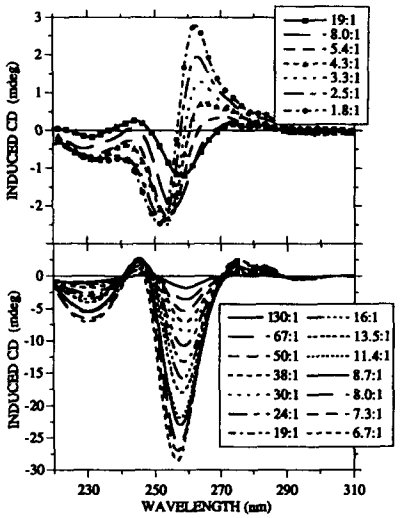

Figure 6. CD spectra of anthracene-9-carbonyl-N^1-spermine–AT complexes at low (upper panel) and high (lower panel) DNA base to ligand ratios. The spectra in each panel were obtained in separate experiments using, for the spectra in the upper panel, 130 μM AT and, for those in the lower panel, 170 μM AT. In each case solutions were 5 mM in NaCl and 1 mm pathlengths were used. The DNA base:ligand ratios are given in the figure inserts.

The ICD of **3** with AT apparently has an essentially constant spectral form at low ligand concentration (Fig. 6, lower panel). However, closer inspection of the data show that the ICD is constantly changing as a function of ligand concentration; there are, for example, no isosbestic points, and the minimum at about 259 nm gradually moves to a shorter wavelength. The much more obvious spectral changes at higher ligand concentrations is shown in the upper panel of Figure 6. These spectra are very excitonic in appearance and the 262 nm intensity is increasing faster than the ligand concentration, suggesting an anthracene–anthracene exciton interaction.

The behaviour of the complex of **3** with AT is in striking contrast to the complex with GC, where the ICD spectra retain a similar form at all mixing ratios until the onset of condensation.[33] This suggests different binding models for **3** with the two homopolymers and is further discussed below. We also note that the ICD of the ctDNA–**3** complex[34] is smaller than that for **3** with GC or AT and, at low ligand concentrations, is essentially an average of the two homopolymer ICD spectra (the homopolymer spectra are opposite in sign under these conditions). The ctDNA–**3** complex retains essentially the same spectral form until mixing ratios of 5:1, whereupon it begins to follow the AT–**3** ICD.

Computer modelling

In describing the results of computer modelling of the complexes of **3** with AT and GC, we recall that the basic approach involves a simple molecular dynamics simulation in which the ligand is free to move over the surface of a fixed conformation 18mer GC or AT-alternating helix including zero, one or two intercalation sites. In certain calculations, two ligands were included. The value of this approach is that it permits the ligand freely to locate favourable binding sites with each helix, rather than relying on ligand placement based on preconceived ideas of the likely sites. We are then able to extract examples of typical binding locations and subject them to further computational studies.

Simulations of a single ligand of **3** with AT and with GC (no intercalation site) provided a general indication of possible ligand locations. With AT, **3** predominantly occupied a location in the minor groove, with the spermine moiety in an essentially all *trans* conformation. With the spermine so located, conformational restrictions within the ligand prevent the anthracene moiety from occupying the groove with its long axis parallel to the groove walls (which presumably would be most favourable; consider the binding of, for example, Hoechst 33258 in the DNA minor groove[42,43]). Instead, the anthracene is located with its long axis orthogonal to the groove (Fig. 7(a)). Prior to moving into the minor groove, the ligand did adopt some transient locations with the spermine moiety lying along the DNA backbone toward the major

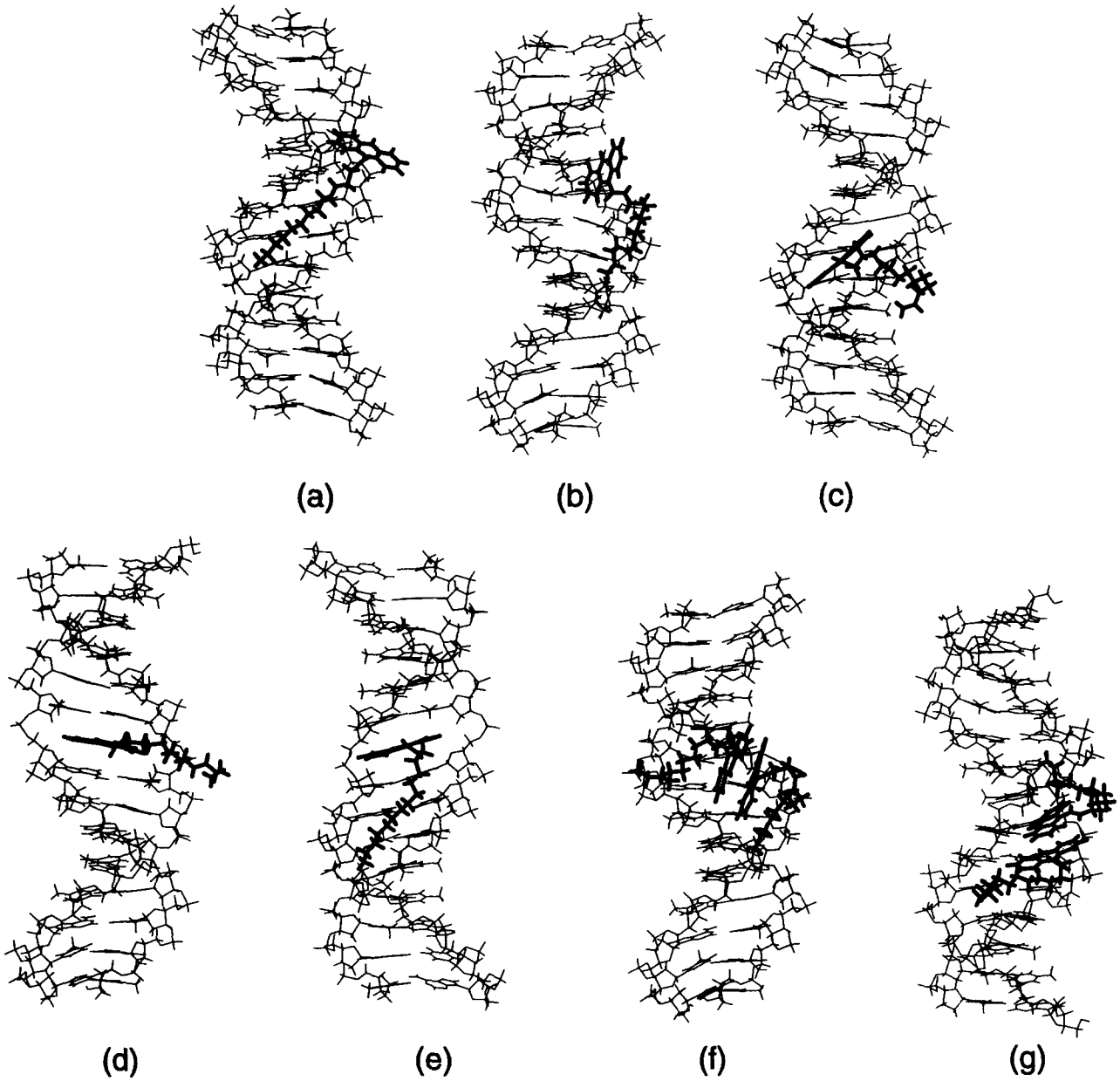

Figure 7. DNA complexes of anthracene-9-carbonyl-N^1-spermine (**3**) generated during molecular dynamics simulations. With the exception of (g), the structures shown are minimized $(dAdT)_7$·$(dAdT)_7$–ligand complexes based on conformations extracted from the dynamics simulations. The structure in (g) was manually constructed prior to minimization.

groove with the anthracene moiety aligned with the major groove (Fig. 7(b)). With GC, the spermine moiety of **3** retained a major groove or major groove backbone location (as in Fig. 7(b)) over the entire simulation. In addition, we observed a further variant, in which the anthracene moiety is minor groove bound with its long axis parallel to the groove and the spermine moiety is wrapped around the helix backbone (Fig. 7(c)). At no time did the spermine enter the GC minor groove.

As it is clear from the spectroscopic data that intercalation is the most important form of binding, we went on to perform simulations with DNA helices including either a single, centrally placed intercalation site, or two spaced intercalation sites positioned towards the ends of the helix. In understanding the data obtained from such simulations, it is necessary to appreciate that only fixed intercalation sites are present. In 400 ps of simulation, one might not necessarily expect intercalation to occur.

In the GC–**3** simulation, intercalation into the single site helix did not occur in the 400 ps window. However, similar ligand orientations occurred to those observed above for the GC–**3** simulation. We emphasize that at no time during either simulation did **3** adopt an orientation with the spermine moiety bound in the GC minor groove. When we used two ligands with GC, we did observe an intercalation event from the major groove after about 200 ps. Once again, we saw no evidence of minor groove binding of the spermine moiety in this simulation. Finally, we performed a fourth simulation using the GC helix and two ligands. Again no minor groove spermine binding was obtained. We did, however, observe an interesting new form of binding in which the spermine moieties lie along the backbone of the major groove and orientate the anthracenes towards each other, causing them to stack. This mode is of interest, considering the excitonic nature of the CD spectra at high ligand concentrations. Although we observed the stacked orientation with the GC helix, there seems no particular reason why it should not also occur with AT. We return to this binding mode below.

In the first simulation of **3** with an AT helix containing a single intercalation site, we observed almost immediate intercalation of the anthracene moiety from the major groove, with the spermine essentially backbone bound (Fig. 7(d)). This location was then retained over the remainder of the trajectory. However, we were concerned that the ligand was initially located adjacent to (although 15 Å from) the major groove intercalation site and that perhaps the observed motion was a function of the starting position. In a second simulation, using a different ligand starting position, we observed motion of the ligand across the DNA for close to 300 ps, followed by intercalation from the minor groove, as shown in Figure 7(e). A measure of the motion of the ligand during this simulation is shown in Figure 8. Here, we have recorded the distances from the spermine moiety (specifically from the midpoint between the secondary amine nitrogen atoms) to the adenine N6 and H2 atoms (which are located centrally in the major groove and minor groove respectively) of the closest base pair to the spermine moiety at each point of the simulation. Following an initial equilibration period, the ligand adopted a major groove location (period (a), Fig. 8), that, in this particular simulation, did not result in intercalation. The spermine moiety then moved to the backbone (period (b), Fig. 8). During this time the anthracene moiety was located in the minor groove, in a location similar to that shown in Figure 7(c). Then, at about 300 ps, the dramatic reduction in distance to the minor groove reference atom (H2) is a consequence of intercalation of the anthracene moiety from the minor groove. Given these results, we conclude that **3** may intercalate with AT from either groove and, in a third simulation, using two intercalation sites and two ligands, we observed intercalation from the major groove after a long period of random motion over the helix surface.

In an attempt to determine relative energies for the different binding modes, we subjected them to energy minimization. Given the flexible and highly charged nature of polyamines, it is difficult to envisage a single, global minimum and we do not want to give the impression that this is the case. Further, given the

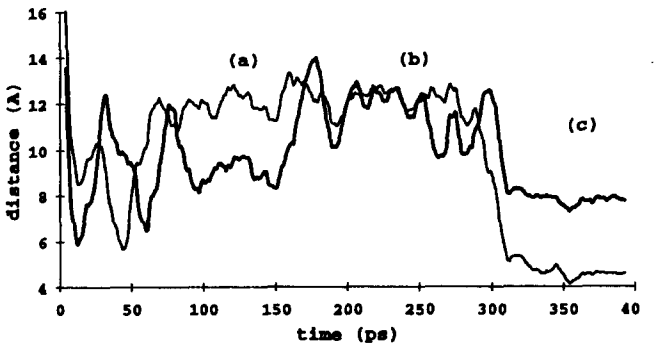

Figure 8. Motion of anthracene-9-carbonyl-N^1-spermine (**3**) in a 400 ps molecular dynamics simulation of its complex with AT. The figure shows the distance from the midpoint between the secondary amine nitrogen atoms of the spermine moiety and the reference atoms (N6 and H2 of adenine) in the DNA major and minor grooves respectively, using the atoms in the nearest base pair to the spermine moiety at each point in the trajectory. The bolder line is the distance to the major groove reference atom. The regions (a) and (b) are further discussed in the text. The rapid reduction in distances at about 300 ps reflects simulation of ligand intercalation from the minor groove. In region (c) the ligand retains this intercalated location.

likely entropic effects present in binding a part hydrophobic, part highly charged molecule like spermine conjugate **3** to DNA, we cannot ascribe too much confidence to a single, computed binding energy which does not take account of these effects. Nevertheless, we were able to show that the minor groove intercalated mode (Fig. 7(e)) was favoured (by some 20 kcal mol^{-1}) over the major groove intercalated mode for AT, whilst for GC these two binding modes were almost identical, energetically. Given the experimental results, this suggests a tendency of the calculation to over-stabilize the spermine–minor groove interaction (and, by extension, the charge–charge interactions between the spermine and the phosphate). This is perhaps to be expected in the absence of explicit water molecules.

The spontaneous occurrence of a two ligand (nominally high ligand concentration) complex in which anthracene–anthracene stacking occurs was an intriguing result. This is indicative of a strong anthracene–anthracene interaction, even in the absence of explicit water molecules. Whilst this complex only occurred in the major groove, we also considered the possibility of an equivalent minor groove complex. A precedent for such binding exists in the observation of a similar two ligand distamycin–DNA complex.[44] Such a complex requires widening of the minor groove to accommodate the two anthracene moieties and therefore could not occur in a rigid helix simulation. The minor groove complex (with AT) was constructed manually and then minimized under similar conditions to an AT–**3**/**3** major groove complex, constructed from ligand orientations obtained in the dynamics simulation. These two complexes (Fig. 7(f) and Fig. 7(g), major and minor groove respectively) were energetically somewhat similar. As the anthracene environment in the minor groove is considerably more hydrophobic (an effect that is likely to be underestimated in these calculations), this location may be favoured in reality.

Thermal denaturation

The UV melting curves and the derivative curve for the melting of ctDNA with **1**, **2** and **3** are shown in Figure 9. Two transitions are present for the ctDNA–**3** complex, one at a lower temperature than T_m for the free DNA, and the other at a higher temperature. As the T_m for a ligand–DNA complex is likely to be higher than for the free DNA, we can assume that the first transition is a pre-melting transition associated with a DNA conformational change. Close inspection of the derivative curve for the ctDNA–**2** complex also suggests a small pre-melting transition occurs. Melting curves for AT with **1**, **2** and **3** are shown in Figure 10. In the complex with **3**, a pre-melt transition is observed as for ctDNA. In addition, a large post-melt transition also occurs. This transition may also be present for ctDNA, but at temperatures above 100 °C. Such a post-melt transition occurs for an ethidium bromide–AT complex (data not shown) and presumably relates to base unstacking in the single-stranded DNA, perhaps when the ligand dissociates. Interestingly, both pre-melt and post-melt transitions also occur for the AT–**2** complex, although, as for the ctDNA pre-melt transition, these are much smaller effects compared to those for **3**. For **1**, the effect, if present, is too small to be observed, even in the derivative curves. Transition temperatures for the systems are given in Table 2, with those of equivalent ethidium complexes for comparison. For both **2** and **3**, the increase in T_m in the complex is greater for AT than for ctDNA. However, it is of note that the increase for ctDNA is larger for the complex with **3**, whilst that for AT is larger for the complex with **2**.

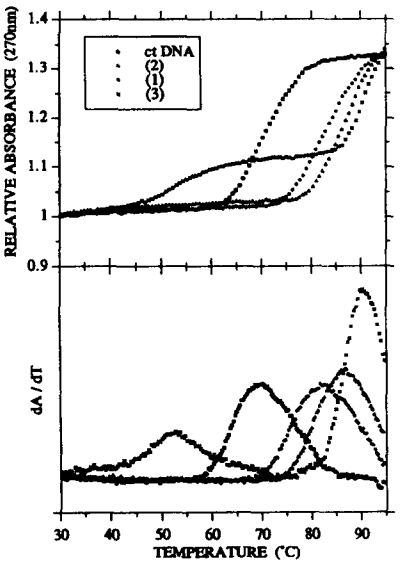

Figure 9. UV melting curves and first derivative curves for the complexes of 20 μM spermidine (**1**), 20 μM spermine (**2**) and 20 μM anthracene-9-carbonyl-N^1-spermine (**3**) with 200 μM ctDNA. Solutions 10 mM in NaCl and pathlengths of 1 mm were used.

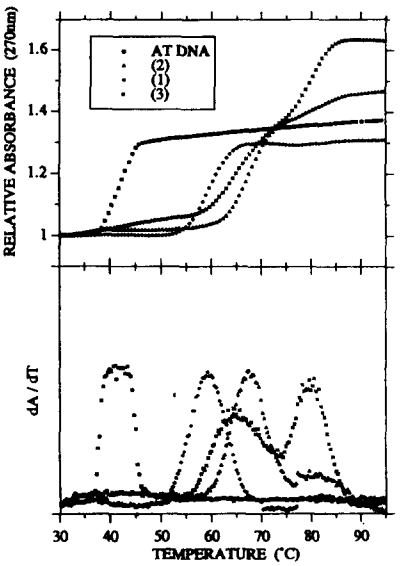

Figure 10. UV melting curves and first derivative curves for the complexes of 20 μM spermidine (**1**), 20 μM spermine (**2**) and 20 μM anthracene-9-carbonyl-N^1-spermine (**3**) with 200 μM AT. Solutions 10 mM in NaCl and pathlengths of 1 mm were used.

Table 2. Transition temperatures (°C) for DNA complexes of spermidine (1), spermine (2), anthracene-9-carbonyl-N^1-spermine (3) and ethidium bromide. Note that only transitions occurring below 100 °C were measured

DNA	ligand	pre-melt	T_m	post-melt	ΔT_m [b]
ctDNA	none		69		-
ctDNA	(1)		82		13
ctDNA	(2)	~40	86		17
ctDNA	(3)	52	90		21
ctDNA	ethidium	38 (?)	88		19
AT	none		42		-
AT	(1)		59		17
AT	(2)	~37	68	82	26
AT	(3)	~40	65	80	23
AT	ethidium	61 [a]	78		36

[a] Shoulder on main transition peak in first derivative curve.
[b] The increase in melting transition temperature, relative to the free DNA.

Discussion

The combination of fluorescence and dichroism data, interpreted in the light of computer-generated binding models, allows us to draw some conclusions regarding the nature of the binding of anthracene-9-carbonyl-N^1-spermine **3** to DNA, and how base sequence might influence this binding. This postulated binding model can then be contrasted with that of spermine, as the main motivation behind studying the DNA complexes of **3** is because **3** is a spectroscopically 'visible' spermine derivative. However, we stress that any conclusions drawn from this data regarding the binding of free spermine to DNA must be viewed with some caution, since the inclusion of an anthracene moiety will influence the overall binding properties of the ligand, and could conceivably change these significantly, compared to spermine itself.

Previous CD data[33] have provided us with a site size for the most favourable binding site with GC and AT (that occupied at low ligand concentrations) of about 8 bases, with the binding to GC being more favourable. The fluorescence quenching and LD data for the GC complex show this to be an intercalative mode, and this is supported by computer modelling, which suggests intercalation from the major groove. As the site size from the fluorescence quenching is in good agreement with the CD data, it seems likely that this is the only intercalation mode of any significance. Hence, **3** probably intercalates from the GC major groove, with the polyamine moiety moving freely in and out of the groove, to and from the backbone. This mode dominates at all ligand concentrations and no evidence of a groove-bound anthracene was obtained until this mode is saturated. Groove binding occurs with GC once this mode is full.

For AT, the situation is more complex. Whilst the LD spectra suggest that essentially only intercalative binding occurs up to relatively high ligand concentrations, CD shows this to comprise a mixture of intercalative binding modes, even at fairly low ligand concentrations. The different site sizes computed from fluorescence enhancement and CD support this. This contrast with GC is mirrored by the computer simulations, in which intercalation from both grooves was observed. The minor groove mode may be more favourable, but the major groove mode is apparently of comparative significance.

At high ligand concentrations, the LD spectra suggest anthracene groove binding occurs with AT and ctDNA. From the CD data, it seems that anthracene–anthracene stacking may be important under such conditions. These interactions could occur in either the minor or major grooves and the single ligand binding geometries shown in Figure 7(b) and Figure 7(c) might be precursors of the double-ligand complexes in the major and minor grooves respectively (Fig. 7(f) and Fig. 7(g)), in addition to being precursors to intercalated complexes at lower ligand concentrations. The ligand location shown in Figure 7(c) is also similar to that recently observed for a distamycin–polyamine conjugate.[45] The single-ligand binding mode in which the spermine moiety occupies the minor groove (Figure 7(a)), may also be a pre-intercalation form of binding, as the ligand occupies a site size equal to that for minor groove intercalation and there is no apparent reason why the anthracene moiety should not ultimately intercalate. This binding mode would be much more favourable with AT than with GC.

The effect of **3** on GC is to reduce the helix orientation in the LD spectra, whilst for AT it seems that the opposite effect is occurring, although this latter effect needs to be verified with further experiments. Given this, and the apparently stronger binding of **3** to GC, compared to AT, the behaviour for ctDNA is qualitatively what would be expected. Hence, at low ligand concentrations, the ctDNA orientation is reduced, but this rate of decrease in orientation drops as a function of ligand concentration until, at very high ligand concentration, some relative increase in orientation is observed. This may be due to initial binding to GC-rich sites and, as these sites fill up, increased occupation of the AT sites. The initial binding to GC-rich sites followed by occupation of AT-rich sites is somewhat similar to the behaviour of free spermine with ctDNA, particularly as described by Marquet and Houssier,[12] and further discussed in Haworth *et al.*,[46] although it should be noted that the

effect of spermine, as observed by electric dichroism relaxation,[12] is to stiffen GC and bend AT,[12] which is totally opposite to the effect of **3**.

In extrapolating the behaviour to the free spermine interaction with DNA, we consider the probable groove location of spermine and the relative binding strengths with GC and AT sequences. From the data describing binding of **3** with ctDNA, we propose a pattern of occupation of GC-rich sites first, consistent with previous studies suggesting the spermine complex with GC sequences to be stronger than that with AT[27] or random sequence DNA.[28] From purely electrostatic arguments, it seems logical to place spermine in an AT minor groove and a GC major groove. The former location is suggested by the photochemical cleavage data of Schmid and Behr,[29] whilst Marquet and Houssier[12] have provided evidence for spermine interaction with the GC bases in the major groove. In structures of several known protein–DNA complexes lysine and arginine residues are found interacting with GC-rich major grooves (as in, for example, the DNA complex of the zinc finger protein Zif268[47]) or AT-rich minor grooves (as in the DNA complex of the engrailed homeodomain[48]).

Our results with the GC–**3** and AT–**3** complexes follow this trend. For GC, we have evidence only for intercalation from the major groove, whereas for AT we suspect that the most favourable intercalation mode occurs from the minor groove, although some major groove binding seems to occur. It should be emphasized when describing this picture of spermine–DNA complexation that the kinetics of spermine association/dissociation are very rapid. Hence, when we describe binding sites, we are really referring to locations that are occupied for a greater percentage of time than would be expected for a completely random complexation model, rather than implying a specific site occupied to the exclusion of all others.

Acknowledgements

This work was supported by a grant from the N.C.I. (CA64299-01) to I.S.H and by grants from the M.R.C. (G9219146N) and the Nuffield Foundation (SCI/180/91/15/G) to I.S.B. We thank Harriet Latham (Oxford University) for technical assistance with the fluorescence and melting experiments.

References

1. Heby, O.; Persson, L. *T.I.B.S.* **1990**, *15*, 153.

2. *The Biology and Chemistry of Polyamines, ICSU Symposium Series*, Vol. 12, Goldemberg, S. H.; Algranati, I. D., Eds; 1989.

3. Koza, R. A.; Herbst, E. J. *Biochem. J.* **1992**, *281*, 87.

4. Basu, H. S.; Feuerstein, B. G.; Deen, D. F.; Lubich, W. P.; Bergeron, R. J.; Samejima, K.; Marton, L. J. *Cancer Res.* **1989**, *49*, 5591.

5. Sarhan, S.; Seiler, N. *Biol. Chem. Hoppe-Seyler* **1989**, *370*, 1279.

6. Basu, H. S.; Pellarin, M.; Feuerstein, B. G.; Shirahata, A.; Samejima, K.; Deen, D. F.; Marton, L. J. *Cancer Res.* **1993**, *53*, 3948.

7. Basu, H. S.; Schwietert, H. C. A.; Feuerstein, B. G.; Marton, L. J. *Biochem. J.* **1990**, *269*, 329.

8. Hougaard, D. M.; Lars, B.; Fujiwara, K.; Larsson, L.-J. *Eur. J. Cell. Biol.* **1987**, *44*, 151.

9. Colson, P.; Houssier, C. *FEBS Lett.* **1989**, *257*, 141.

10. Smirnov, I. V.; Dimitrov, S. I.; Makarov, V. L. *J. Biomol. Struct. Dyn.* **1988**, *5*, 1149.

11. Basu, H. S.; Sturkenboom, M. C. J. M.; Delcros, J.-G.; Csokan, P. P.; Szollosi, J.; Feuerstein, B. G.; Marton, L. J. *Biochem. J.* **1992**, *282*, 723.

12. Marquet, R.; Houssier, C. *J. Biomol. Struct. Dyn.* **1988**, *6*, 235.

13. Marquet, R.; Houssier, C.; Fredericq, E. *Biochim. Biophys. Acta* **1985**, *825*, 365.

14. Rich, A. *Gene* **1993**, *135*, 99.

15. Pohl, F. M.; Jovin, T. M. *J. Mol. Biol.* **1972**, *67*, 375.

16. Behe, M.; Felsenfeld, G. *Proc. Natl Acad. Sci U.S.A.* **1981**, *78*, 1619.

17. Chen, H. H.; Behe, M. J.; Rau, D. C. *Nucl. Acids Res.* **1984**, *12*, 2381.

18. Thomas, T. J.; Messner, R. P. *J. Mol. Biol.* **1988**, *201*, 463.

19. Chiu, S. K.; Rao. B. J.; Story, R. M.; Radding, C. M. *Biochemistry* **1993**, *32*, 13146.

20. Hampel, K. J.; Crosson, P.; Lee, J. S. *Biochemistry* **1991**, *30*, 4455.

21. Bancroft, D.; Williams, L. D.; Rich, A.; Egli, M. *Biochemistry* **1994**, *33*, 1073.

22. Drew, H. R.; Dickerson, R. E. *J. Mol. Biol.* **1981**, *151*, 535.

23. Jain, S.; Zon, G; Sundaralingam, M. *Biochemistry* **1989**, *28*, 2360.

24. Williams, L. D.; Frederick, C. A.; Ughetto, G.; Rich, A. *Nucleic Acids Res.* **1990**, *18*, 5533.

25. Padmanabhan, S.; Brushaber, V. M.; Anderson, C. F.; Record, Jr M. T. *Biochemistry* **1991**, *30*, 7550.

26. Wemmer, D. E.; Srivenugopal, K. S.; Reid, B. R.; Morris, D. R. *J. Mol. Biol.* **1985**, *185*, 457.

27. Stewart, K. D. *Biochem. Biophys. Res. Commun.* **1988**, *152*, 1441.

28. Winkle, S. A.; Crooks, P. A. *J. Pharm. Pharmacol.* **1988**, *40*, 809.

29. Schmid, N; Behr, J.-P. *Biochemistry* **1991**, *30*, 4357.

30. Basu, H. S.; Shafer, R. H.; Marton, L. J. *Nucleic Acids Res.* **1987**, *15*, 5873.

31. Vertino, P. M.; Bergeron, R. J.; Cavanaugh, Jr P. F.; Porter, C. W. *Biopolymers* **1987**, *26*, 691.

32. Behr, J.-P. *J. Chem. Soc., Chem. Commun.* **1989**, 101.

33. Rodger, A.; Blagbrough, I. S.; Adlam, G.; Carpenter, M. L. *Biopolymers* **1994**, *34*, 1583.

34. Adlam, G.; Blagbrough, I. S.; Taylor, S.; Latham, H. C., Haworth, I. S.; Rodger, A. *Bioorg. Med. Chem. Lett.* **1994**, *4*, 2435.

35. Zegar, I. S.; Prakash, A. S.; Harvet, R. G.; Lebreton, P. R. *J. Am. Chem. Soc.* **1985**, *107*, 7990.

36. Denny, W. *Anti-Cancer Drug Des.* **1989**, *4*, 241.

37. Pearlman, D. A.; Case, D. A.; Caldwell, J. C.; Seibel, G. L.; Singh, U. C.; Weiner, P.; Kollman, P. A. AMBER 4.0, University of California, San Francisco, 1991.

38. Weiner, S. J.; Kollman, P. A.; Nguyen, D. T.; Case, D. A. *J. Comp. Chem.* **1986**, *7*, 230.

39. Dewar, M. J. S.; Zoebisch, E. G.; Healy, E. F.; Stewart, J. J. P. *J. Am. Chem. Soc.* **1985**, *107*, 3902.

40. RATTLER, Oxford Molecular Ltd, Oxford Science Park, Oxford, U.K.

41. Heller, D. P.; Greenstock, C. L. *Biophys. Chem.* **1994**, *50*, 305.

42. Pjura, P. E.; Grzeskowiak, K.; Dickerson, R. E. *J. Mol. Biol.* **1987**, *197*, 257.

43. Teng, M.-K.; Usman, N.; Frederick, C. A.; Wang, A. H.-J. *Nucleic Acids Res.* **1988**, *16*, 2671.

44. Pelton, J. G.; Wemmer, D. E. *Proc. Natl Acad. Sci U.S.A.* **1989**, *86*, 5723.

45. Blasko, A.; Browne, K. A.; Bruice, T. C. *J. Am. Chem. Soc.* **1994**, *116*, 3726.

46. Haworth, I. S.; Rodger, A.; Richards, W. G. *Proc. Royal Soc. Lond. B* **1991**, *244*, 107.

47. Pavletich, N. P.; Pabo, C. O. *Science* **1991**, *252*, 809.

48. Kissinger, C. R.; Liu, B. S.; Martin-Blanco, E.; Kornberg, T. B.; Pabo, C. O. *Cell* **1990**, *63*, 579.

49. *Handbook of Chemistry and Physics*, 65th Edition, p. C-29, Weaste, R. C.; Astle, M. J.; Beyer, W. H., Eds; CRC Press, Boca Raton, Florida, 1984–1985

(*Received in U.S.A.* 5 *December* 1994; *accepted* 28 *March* 1995)